Nanoporous Gas Transport In Shale Gas Reservoirs

Evans Ogoun
Robert Gordon University, United Kingdom

Priscilla Ogunlude
Robert Gordon University, United Kingdom

Ofasa Abunomah
Robert Gordon University, United Kingdom

Edward Gobina
Robert Gordon University, United Kingdom, e.gobina@rgu.ac.uk

Abstract: In more conventional gas reservoirs, gas flow is simple, uncomplicated, and described by simple flux pressure drop expressions. In shale reservoirs however, this relationship takes the form of a more complex and multiscale flow process involving special flow mechanisms. Shale gas reservoirs often contain a significant number of nanopores leading to an apparent permeability that depends on pore fluid type, pore structure and pressure differentials. The complex geometry of shale reservoirs has drastically stimulated basic research on the transport mechanisms involved in the extraction of gas from shale formations. This study is aimed at studying the gas flow in nano pores. In this paper, permeation experiments for methane flow through nanoporous membranes were conducted and the effect of the pore size and pressure on the behaviour of the gas was analysed. The results obeyed the criteria to divide the flow stage into Darcy and Non-Darcy flow. As the pressure increases, the reservoir permeability also increases, and the gas tends to move faster thereby increasing the rate at which it flows per unit area in the system regardless of the temperature difference which means pressure gradient establishes the direction and rate of flow of gas in a reservoir.

Keywords: Shale gas, Nanopores, permeability, Darcy Law, Knudsen diffusion

Introduction

Natural gas account for a large percentage for the global increase in the demand for energy in recent times, this has necessitated the rapid growth in the production of unconventional gas reservoirs in United States of America, China, and the Middle East. The advancement in producing from unconventional oil and gas fields such as shale gas in recent decades has given rise to new opportunities and complex technical innovations in the oil and gas sector. These new frontiers have cumulated to a greater concentration on the reservoir petrophysical properties and heterogeneities that affect the performance of natural gas reservoir (Siddharth et al 2019). Natural gas plays two distinctive roles in ensuring the faster progression to low carbon energy system; this include promoting a move away from coal in fast-emerging economies where demand for energy and other coal uses are rapidly growing and where renewables and other non-petroleum products might not be able to expand rapidly enough to replace coal on their own. According to Yu et al (2016) reservoir rocks being the final product of sequence of complex geological and hydrodynamic events such as weathering, sedimentation, compaction and diagenesis, are defined by complex pore space geometry. This complex pore geometry governs the associated petrophysical parameters like porosity, permeability and fluid saturation, which in turns influence the gas transport mechanism of the reservoir during the process of exploitation.

Shale Gas Reservoir

Shale is a geological rock formation composed of clay minerals derived from fine sediments deposited in calm environments such as the bottom of the sea and lakes, after been buried million years ago. It is traditionally regarded as a potential source rock or seal/cap rock for conventional hydrocarbon reservoirs. But it is recognized as unconventional reservoirs for hydrocarbons in recent times, although with lower permeability and large amount of organic matter than the conventional reservoirs. In shale gas reservoirs, gas typically occurs in two modes; absorbed as organic matter within the shale beds in a similar manner to coal bed methane, and as free gas in porosity within the shale matrix, like conventional reservoirs. The low permeability of shale reservoirs

dictates that specialized technique necessary for the exploration and production (Speight 2013).

The varieties of rock types observed in organic rich shales implies the present of different types of shale gas reservoirs. Each reservoir may have distinctive geochemical and geological characteristics that may require specific methods of drilling, completion, production, resource and reserve evaluation (Cramer 2008). Bustin 2006 pointed out four major properties important in characterizing each shale gas play, which include maturity of the organic matter, the type of gas generated and stored in the reservoir (either biogenic or thermogenic), total organic carbon (TOC) content of the strata, and the permeability index of the reservoir. Shale gas is generated in two different ways: thermogenic and biogenic, although a mixture of gas types is possible. Thermogenic shale gas is generated from the cracking of organic matter or secondary cracking of oil. And biogenic shale gas is generated from microbes in areas of freshwater recharge (Martin et al 2004).

According to Cramer (2008) thermogenic gas is associated with mature organic matters subjected to a relatively intense temperature and pressure in other to generate hydrocarbons. In essence, the more mature the organic matter the higher gas in-place resources that can be generated. The complexity of the geometry of shale reservoirs has drastically stimulated basic research on the transport mechanisms involved in the extraction of gas from shale formations.

Natural Gas Transport Mechanisms

The accelerated exploration and production activities for unconventional gas reservoirs in recent years has drastically stimulated basic research on the flow mechanisms involved from gas extraction, gas storage mechanism and the release of the gas from shale (Sunjay and Govind 2019). Gas flow in some geological formations involves two different physical migration processes, one associated with a distribution network of large-scale natural fractures, and the other related to finer porous structures of matrix blocks within the structure. The gas movement through the large-scale fractures is termed permeability flow, which is described by Darcy's law with pressure gradient as the main driven force. While the movement of gas through the matrix blocks is known as molecular diffusion processes, which occurs as a result of several different mechanisms subject to pore size distribution and are described using Fick's law (Sunjay and Govind 2019).

For a low permeability and pressure system where the pore size distribution is of the same scale with the mean free path of the gas molecules, an enhance diffusion known as the Knudson diffusion occurs (Ziarani and Agus 2012). According to Hildenbrand et al (2012) potential transport mechanisms in shale reservoir formations involve six distinctive flow mechanisms which are convective pressure driven flow, Knudson diffusion, molecular diffusion, surface diffusion, configurational diffusion and liquid diffusion. Under an isothermal condition the transportation of gas in porous media involves the following transport mechanisms viscous flow, Knudson diffusion and molecular diffusion (Yao et al 2013).

Bird et al (2002) described the molecular diffusion as the relative motion of different gas species that occur specifically in multi-component gas transport in porous medium, while Knudson diffusion and viscous flow refers to individual gas species that occurs when gas moves in porous medium. The Knudson diffusion is initiated from collision between molecules and the reservoir pore wall, but the viscous flow results from collision between molecules as shown in Figure 1.
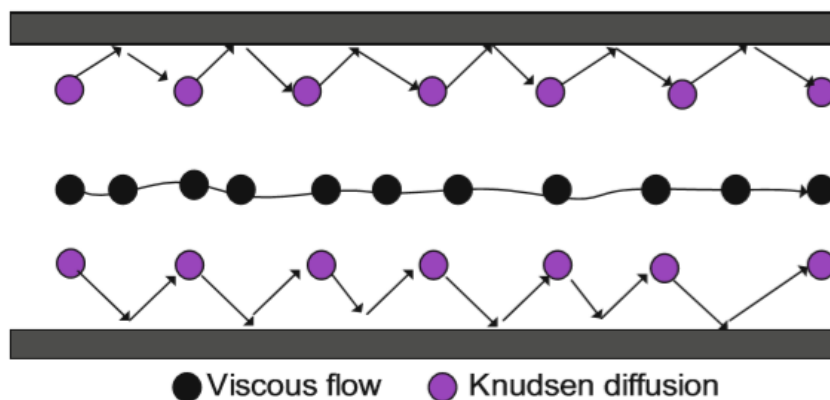

Figure 1. Diagram showing Gas Movement within a Porous Medium (Bird et al 2002)

Javadpour et al (2007) acknowledged a widely recognized dimensionless parameter that described the degree suitable to characterize the flow regimes of gas molecules in porous medium; this continuum model is known as the Knudsen number (K_n); which is the ratio of the molecular mean free path ($Ʌ$) to the length scale L
Where $Ʌ$ is defined as:

$$Ʌ = K_B T / 2\pi\delta^2 P \tag{1}$$

K_B is the Boltkmann constant ($K_B = 1.3805 \times 10^{-23}$), T is temperature in Kelvin and δ is the collision diameter of the gas molecules. Gas transport in porous medium is characterized into four flow regimes with reference to Knudson number (K_n). When the Knudsen number is below 0.001 a continuum flow regime occurs, where the Knudsen number is between 0.001 and 0.1 the slip flow regime occurs, when the Knudsen number is between 0.1 and 10 transition regime occur and free molecular flow regime occurs when the Knudsen is greater than 10 as shown in table 1.1 (Yao et al 2013).

Table 1. Classification of Gas Flow Regimes with Reference to Knudsen Number (Adopted from Yao et al 2013)

Boltzmann Equation			
Navier Stokes equation			
Non-slip condition	Slip condition		
Darcy's law	Slip flow regime	Transition regime	Free molecular regime
Continuum flow regime			
0 ⟶ 0.001 K_n	0.01 — 0.1 ⟶ K_n	0.1 — 10 ⟶ K_n	10 ⟶ ∞ K_n

Experimental Materials and Method

This research adopts the ceramic core technology which can replace conventional techniques in reservoir evaluation. For this study synthetic ceramic cores have been selected as the core materials. They are suitable for this study because of their low cost, low energy usage, durability, and high tensile strength, enhance performance and their mechanical and thermal resistance which does not impede their application in acidic high temperature and present surroundings which are mostly common in the oil and gas industries.

The experiment is set up using the following equipment labelled in figure 2. (1) pressure gauge (2) pressure valve (3) gas regulator (4) gas cylinder (5) thermometer (6) thermocouple transducer (7) flow meter (8) heat regulator (9) heat jacket and (10) core holder.

The system is assembled with a porous ceramic core fitted into the centre of an annulus of a shell and tube mechanism and both ends covered with graphite seal to avoid gas leakage. Prior to each experiment, a leak test is carried out by releasing the feed gas (natural gas) at double the pressure required for the experiment to detect any pressure drop along the lines, and a snoop solution is used to detect any leak.

The system is heated to a desired temperature and allowed to reach thermal stability. Natural gas (CH_4) contained in the gas cylinder is then released via the gas regulator and allowed to flow through the pressure valve into the nano-core sample, which is been held firm by the core holder coated with a heating jacket that serves as a heat absorber. The gas is allowed to flow through the porous core to an exit line from the core inlet along the flow meter outlet to a fume of cupboard where the gas is discharge. The pressure gauge is monitored and regulated to the desired pressure and temperature condition, after which the system is allowed to operate for a period for the reading in the flow meter to stabilize. Once this stability is attained, the reading on the flow meter, pressure gauge and thermocouple are recorded.

This experimental procedure was conducted for three different nano-core samples with pore sizes of 15nm, 200nm and 6000nm at predetermined pressures of 0.2, 0.6, 1.0, 1.4, 1.8, 2.2, 2.6, and 3 bar. The experiment was carried out at an assumed reservoir condition of thermal stability of 100°C, 150°C and 200°C for each of the three different pore size membranes.
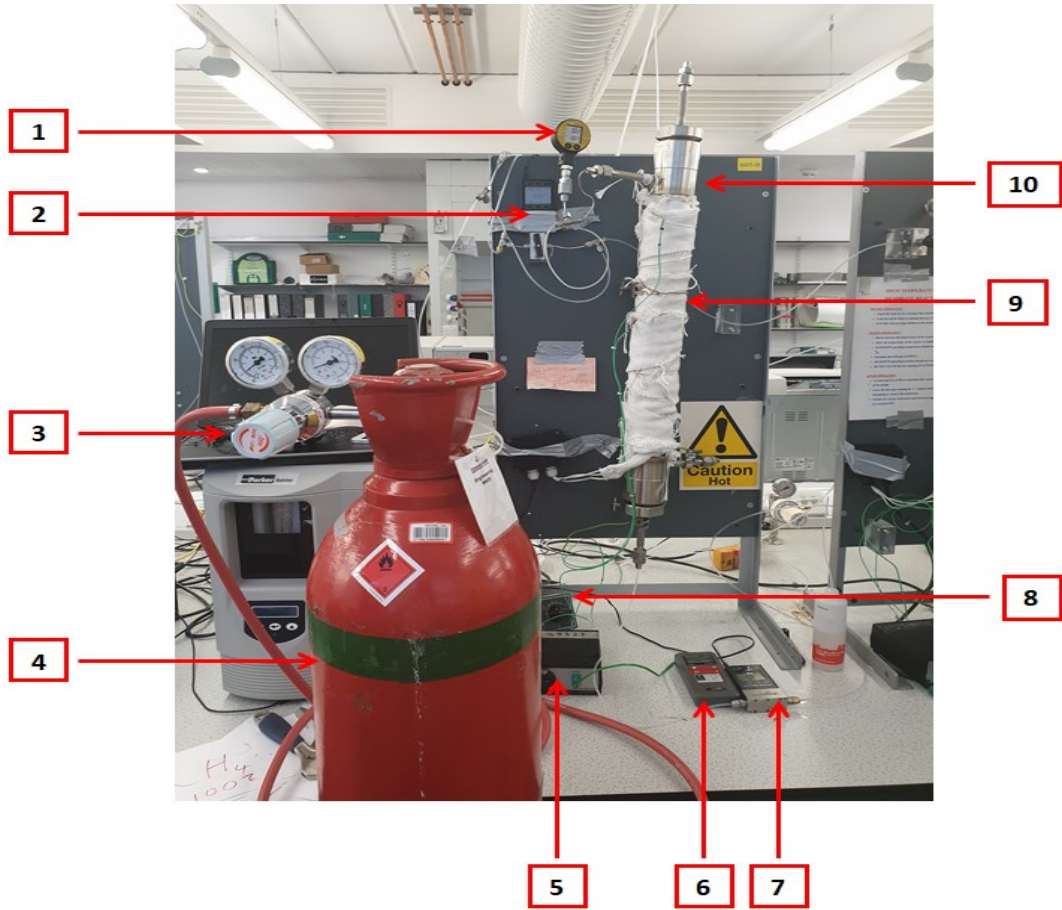
Figure 2. Experimental Set-up showing all Equipment

The flowmeter readings at thermal stability of $100^{\circ}C$, $150^{\circ}C$ and $200^{\circ}C$ for the three different cores and other computed parameters are summarized in Table 2.

Table 2. Summary of the Experimental Results and Parameters

TEMPERATURE 100oC

Inlet pressure (Bar)	Outlet pressure (Bar)	Inlet pressure (Pa)	Outlet pressure (Pa)	Pressure drop (Pa)	Average Pressure (Pa)	Inverse Average Pressure (1/Pa)	CORE: 15NM Flowrate (LPM)	Flowrate (M³/S)	Surface Area (M²)	Flux (M³/M²S)	Permeance (M³/M²S Pa)	CORE:200NM Flowrate (LPM)	Flowrate (M³/S)	Surface Area (M²)	Flux (M³/M²S)	Permeance (M³/M²S Pa)	CORE: 6000NM Flowrate (LPM)	Flowrate (M³/S)	Surface Area (M²)	Flux (M³/M²S)	Permeance (M³/M²S Pa)
1.2	1	120000	100000	20000	110000	9.091E-06	1.34	2.278E-05	5.339	4.267E-06	2.133E-10	1.05	1.785E-05	1.26	1.417E-05	7.083E-10	0.84	1.428E-05	3.112	4.589E-06	2.294E-10
1.6	1	160000	100000	60000	130000	7.692E-06	2.41	4.097E-05	5.339	7.674E-06	1.279E-10	2.02	3.434E-05	1.26	2.725E-05	4.542E-10	1.78	3.026E-05	3.112	9.724E-06	1.621E-10
2	1	200000	100000	100000	150000	6.667E-06	2.84	4.828E-05	5.339	9.043E-06	9.043E-11	2.43	4.131E-05	1.26	3.279E-05	3.279E-10	1.97	3.349E-05	3.112	1.076E-05	1.076E-10
2.4	1	240000	100000	140000	170000	5.882E-06	3.1	0.0000527	5.339	9.871E-06	7.051E-11	2.71	4.607E-05	1.26	3.656E-05	2.612E-10	2.15	3.655E-05	3.112	1.174E-05	8.389E-11
2.8	1	280000	100000	180000	190000	5.263E-06	3.32	5.644E-05	5.339	1.057E-05	5.873E-11	2.93	4.981E-05	1.26	3.953E-05	2.196E-10	2.3	0.0000391	3.112	1.256E-05	6.98E-11
3.2	1	320000	100000	220000	210000	4.762E-06	3.47	5.899E-05	5.339	1.105E-05	5.022E-11	3.1	0.0000527	1.26	4.183E-05	1.901E-10	2.42	4.114E-05	3.112	1.322E-05	6.009E-11
3.6	1	360000	100000	260000	230000	4.348E-06	3.6	0.0000612	5.339	1.146E-05	4.409E-11	3.24	5.508E-05	1.26	4.371E-05	1.681E-10	2.54	4.318E-05	3.112	1.388E-05	5.337E-11
4	1	400000	100000	300000	250000	0.000004	3.73	6.341E-05	5.339	1.188E-05	3.959E-11	3.34	5.678E-05	1.26	4.506E-05	1.502E-10	2.66	4.522E-05	3.112	1.453E-05	4.844E-11

TEMPERATURE 150oC

Inlet pressure (Bar)	Outlet pressure (Bar)	Inlet pressure (Pa)	Outlet pressure (Pa)	Pressure drop (Pa)	Average Pressure (Pa)	Inverse Average Pressure (1/Pa)	CORE: 15NM Flowrate (LPM)	Flowrate (M³/S)	Surface Area (M²)	Flux (M³/M²S)	Permeance (M³/M²S Pa)	CORE:200NM Flowrate (LPM)	Flowrate (M³/S)	Surface Area (M²)	Flux (M³/M²S)	Permeance (M³/M²S Pa)	CORE: 6000NM Flowrate (LPM)	Flowrate (M³/S)	Surface Area (M²)	Flux (M³/M²S)	Permeance (M³/M²S Pa)
1.2	1	120000	100000	20000	110000	9.091E-06	1.37	2.329E-05	5.339	4.362E-06	2.181E-10	1.07	1.819E-05	1.26	1.444E-05	7.218E-10	0.93	1.581E-05	3.112	5.08E-06	2.54E-10
1.6	1	160000	100000	60000	130000	7.692E-06	2.45	4.165E-05	5.339	7.801E-06	1.3E-10	2.01	3.417E-05	1.26	2.712E-05	4.52E-10	1.87	3.179E-05	3.112	1.022E-05	1.703E-10
2	1	200000	100000	100000	150000	6.667E-06	2.88	4.896E-05	5.339	9.17E-06	9.17E-11	2.44	4.148E-05	1.26	3.292E-05	3.292E-10	2.1	0.0000357	3.112	1.147E-05	1.147E-10
2.4	1	240000	100000	140000	170000	5.882E-06	3.15	5.355E-05	5.339	1.003E-05	7.164E-11	2.71	4.607E-05	1.26	3.656E-05	2.612E-10	2.28	3.876E-05	3.112	1.246E-05	8.896E-11
2.8	1	280000	100000	180000	190000	5.263E-06	3.36	5.712E-05	5.339	1.07E-05	5.944E-11	2.94	4.998E-05	1.26	3.967E-05	2.204E-10	2.42	4.114E-05	3.112	1.322E-05	7.344E-11
3.2	1	320000	100000	220000	210000	4.762E-06	3.53	6.001E-05	5.339	1.124E-05	5.109E-11	3.14	5.338E-05	1.26	4.237E-05	1.926E-10	2.55	4.335E-05	3.112	1.393E-05	6.332E-11
3.6	1	360000	100000	260000	230000	4.348E-06	3.68	6.256E-05	5.339	1.172E-05	4.507E-11	3.29	5.593E-05	1.26	4.439E-05	1.707E-10	2.68	4.556E-05	3.112	1.464E-05	5.631E-11
4	1	400000	100000	300000	250000	0.000004	3.8	0.0000646	5.339	1.21E-05	4.033E-11	3.42	5.814E-05	1.26	4.614E-05	1.538E-10	2.8	0.0000476	3.112	1.53E-05	5.099E-11

TEMPERATURE 200oC

Inlet pressure (Bar)	Outlet pressure (Bar)	Inlet pressure (Pa)	Outlet pressure (Pa)	Pressure drop (Pa)	Average Pressure (Pa)	Inverse Average Pressure (1/Pa)	CORE: 15NM Flowrate (LPM)	Flowrate (M³/S)	Surface Area (M²)	Flux (M³/M²S)	Permeance (M³/M²S Pa)	CORE:200NM Flowrate (LPM)	Flowrate (M³/S)	Surface Area (M²)	Flux (M³/M²S)	Permeance (M³/M²S Pa)	CORE: 6000NM Flowrate (LPM)	Flowrate (M³/S)	Surface Area (M²)	Flux (M³/M²S)	Permeance (M³/M²S Pa)
1.2	1	120000	100000	20000	110000	9.091E-06	1.39	2.363E-05	5.339	4.426E-06	2.213E-10	1.08	1.836E-05	1.26	1.457E-05	7.286E-10	0.95	1.615E-05	3.112	5.19E-06	2.595E-10
1.6	1	160000	100000	60000	130000	7.692E-06	2.44	4.148E-05	5.339	7.769E-06	1.295E-10	2.06	3.502E-05	1.26	2.779E-05	4.632E-10	1.93	3.281E-05	3.112	1.054E-05	1.757E-10
2	1	200000	100000	100000	150000	6.667E-06	2.87	4.879E-05	5.339	9.138E-06	9.138E-11	2.48	4.216E-05	1.26	3.346E-05	3.346E-10	2.15	3.655E-05	3.112	1.174E-05	1.174E-10
2.4	1	240000	100000	140000	170000	5.882E-06	3.15	5.355E-05	5.339	1.003E-05	7.164E-11	2.76	4.692E-05	1.26	3.724E-05	2.612E-10	2.35	3.995E-05	3.112	1.284E-05	9.17E-11
2.8	1	280000	100000	180000	190000	5.263E-06	3.38	5.746E-05	5.339	1.076E-05	5.979E-11	2.98	5.066E-05	1.26	4.021E-05	2.234E-10	2.5	0.0000425	3.112	1.366E-05	7.587E-11
3.2	1	320000	100000	220000	210000	4.762E-06	3.56	6.052E-05	5.339	1.134E-05	5.152E-11	3.17	5.389E-05	1.26	4.277E-05	1.944E-10	2.64	4.488E-05	3.112	1.442E-05	6.555E-11
3.6	1	360000	100000	260000	230000	4.348E-06	3.72	6.324E-05	5.339	1.184E-05	4.556E-11	3.33	5.661E-05	1.26	4.493E-05	1.728E-10	2.78	4.726E-05	3.112	1.519E-05	5.841E-11
4	1	400000	100000	300000	250000	0.000004	3.87	6.579E-05	5.339	1.232E-05	4.108E-11	3.46	5.882E-05	1.26	4.668E-05	1.556E-10	2.94	4.998E-05	3.112	1.606E-05	5.353E-11

From Table 2, the inlet and outlet pressures in bar were gotten directly from the experiment and were converted to Pascal (1bar = 100,000pa). Pressure Drop was derived from the difference of the outlet and inlet pressure in Pascal, average pressure was computed by adding the inlet and outlet pressure divided by 2 and the inverse average pressure is 1 divided by the average pressure.

The flowrates were also measured directly from the experiment using the flowmeter in LPM and converted to M^3/S. The surface area for each of the membranes were derived from the equation $2\pi rh + 2\pi hr^2$ (Where, r is the radius of the membrane and h, height which were directly measured in the laboratory). The flux was calculated as the ratio of the flowrate and surface area and finally the permeance was derived as the ratio of flux and pressure drop.

Results

Effect of Pressure Drop on Flux for the Different Membranes at the Different Temperatures
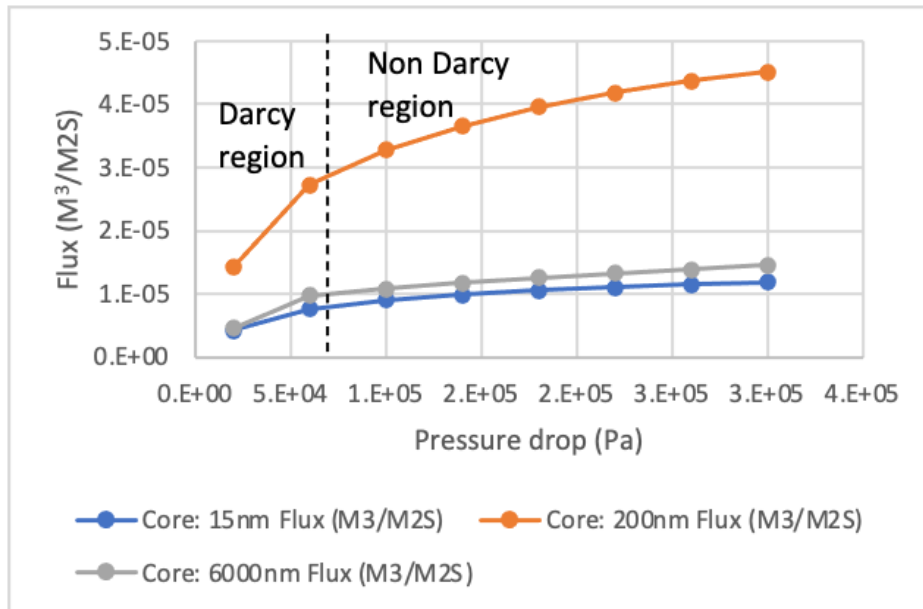
Figure 3. Effect of Pressure Drop on Flux for the Different Membranes at Temperature 100°
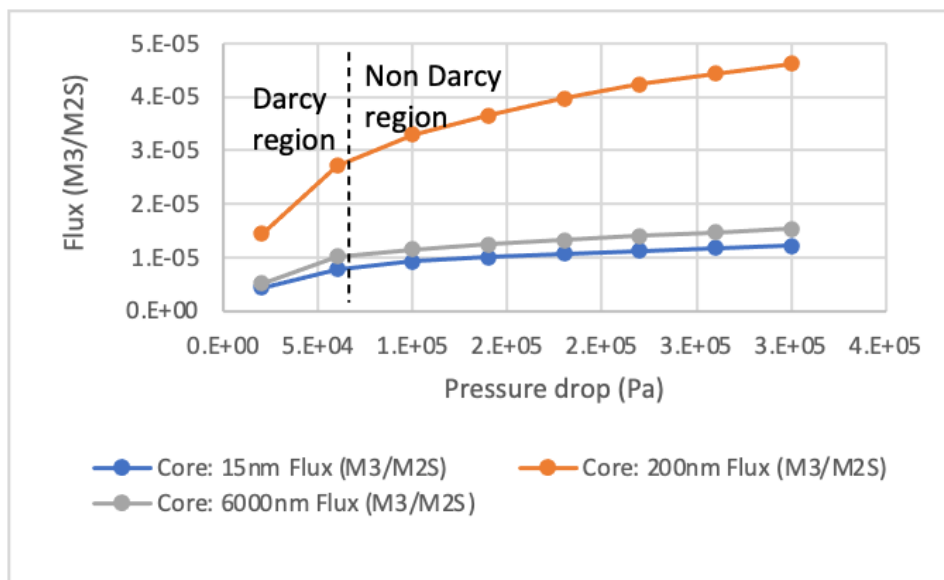
Figure 4. Effect of Pressure Drop on Flux for the Different Membranes at Temperature 150°
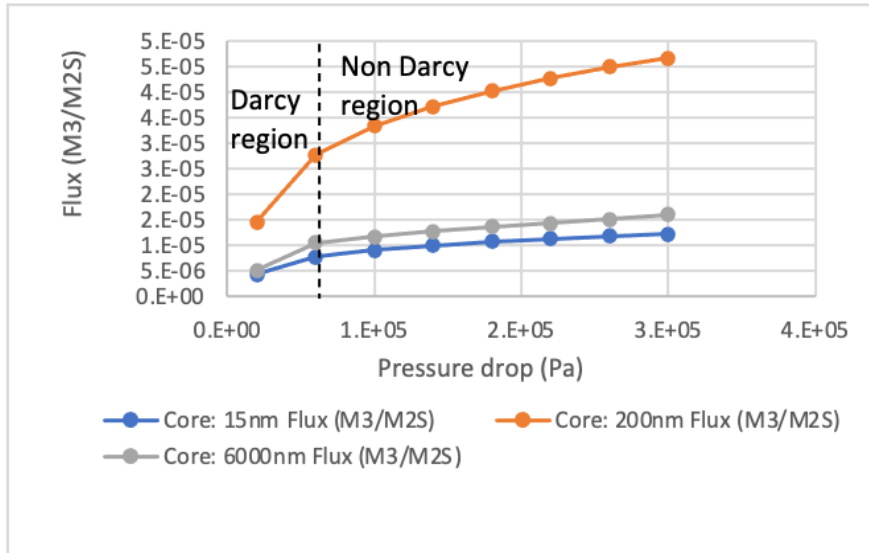
Figure 5. Effect of Pressure Drop on Flux for the Different Membranes at Temperature 200°

Effect of Average Pressure on Permeance for the Different Membranes at the Different Temperatures

Figure 6. Effect of Average Pressure on Permeance for the Different Membranes at Temperature 100°
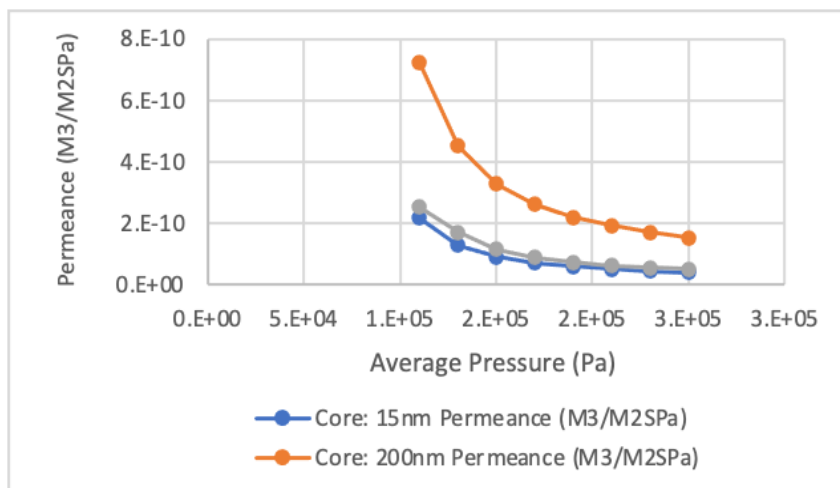

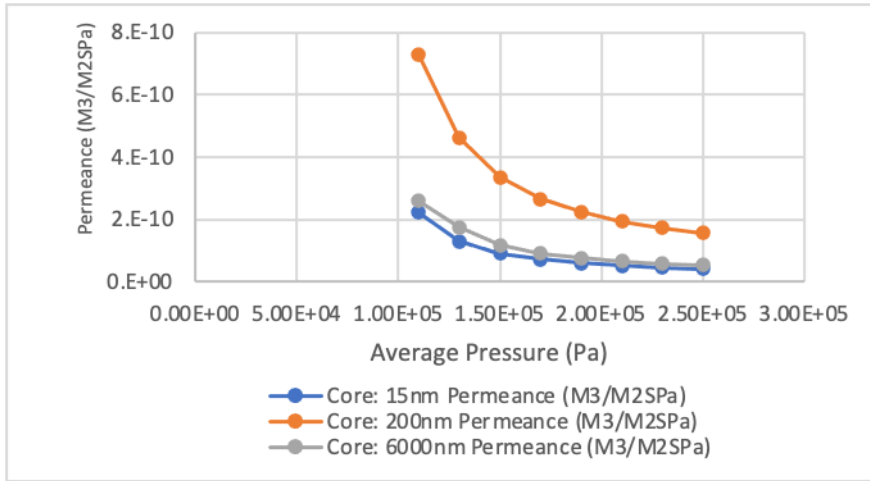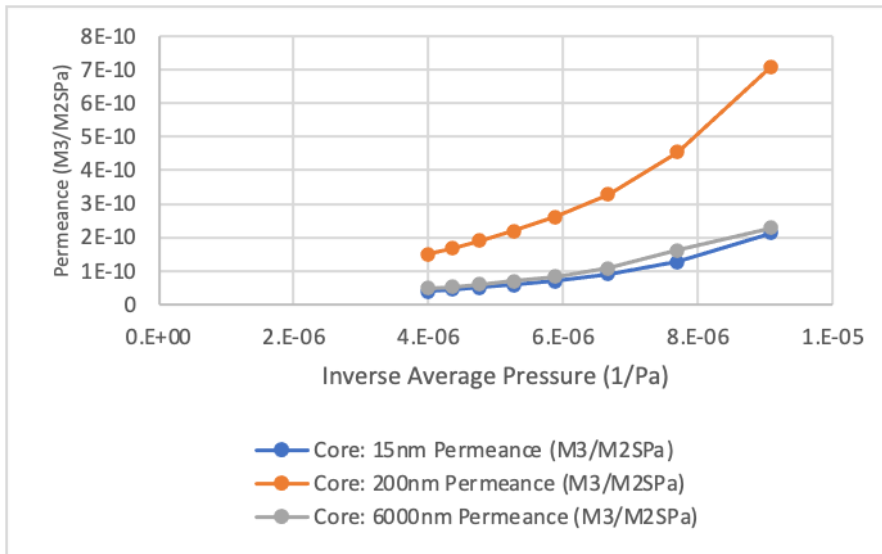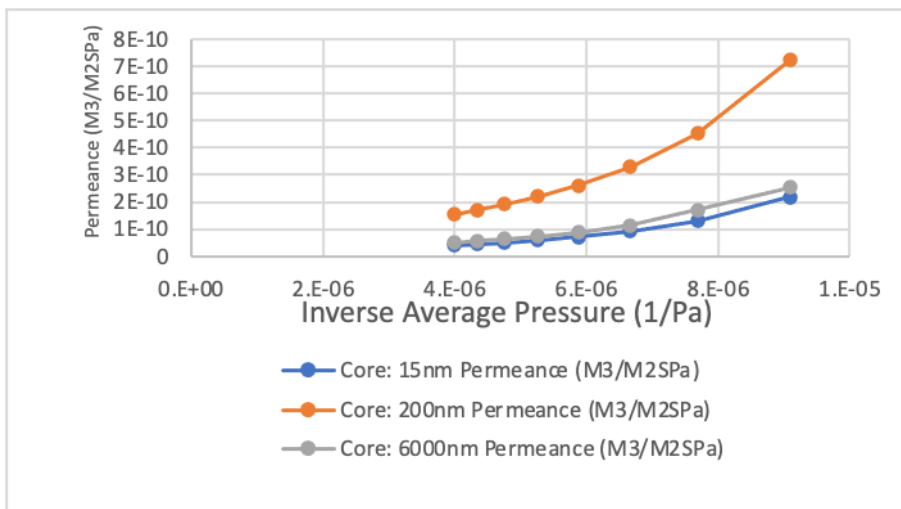Figure 7. Effect of Average Pressure on Permeance for the Different Membranes at Temperature 150°

Figure 8. Effect of Average Pressure on Permeance for the Different Membranes at Temperature 200°

Effect of Inverse Average Pressure on Permeance for the Different Membranes at the Different Temperatures

Figure 9. Effect of Inverse Average Pressure on Permeance for the Different Membranes at Temperature 100°

Figure 10. Effect of Inverse Average Pressure on Permeance for the Different Membranes at Temperature 150°
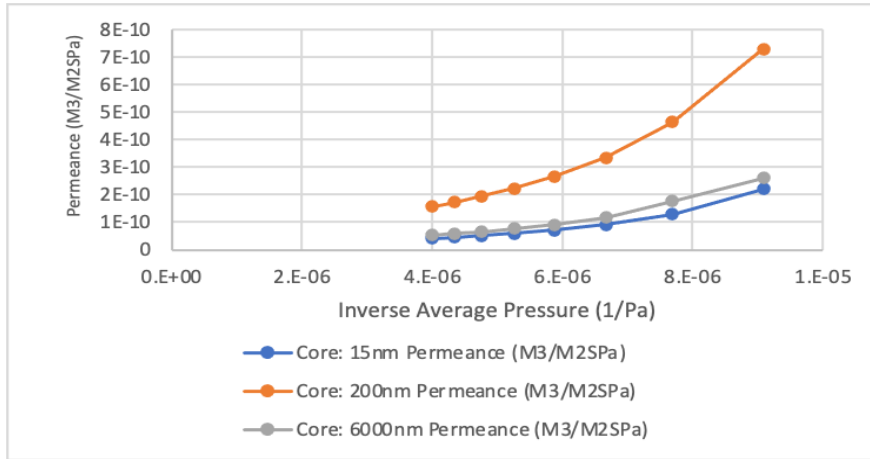
Figure 11. Effect of Inverse Average Pressure on Permeance for the Different Membranes at Temperature 200°

Darcy Law Region Effect of Pressure Drop on Permeance for the Different Membranes at Different Temperatures
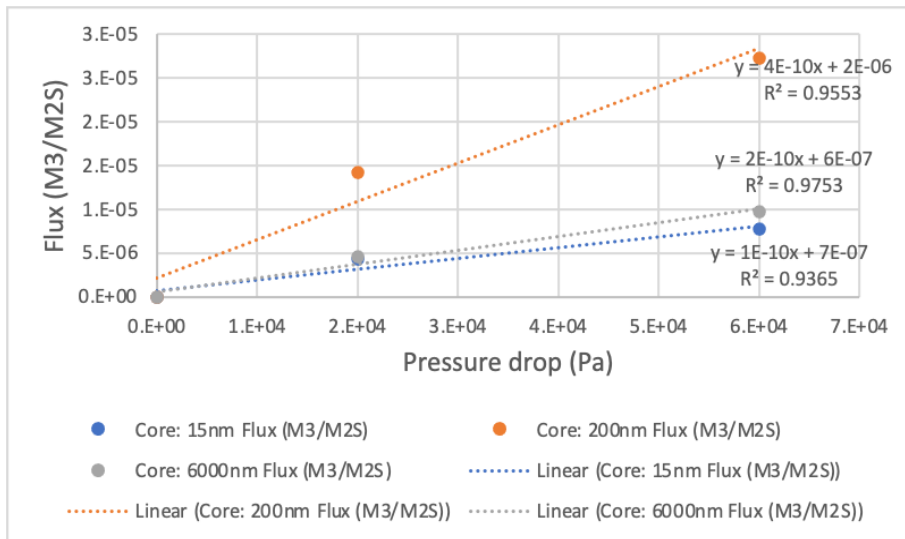

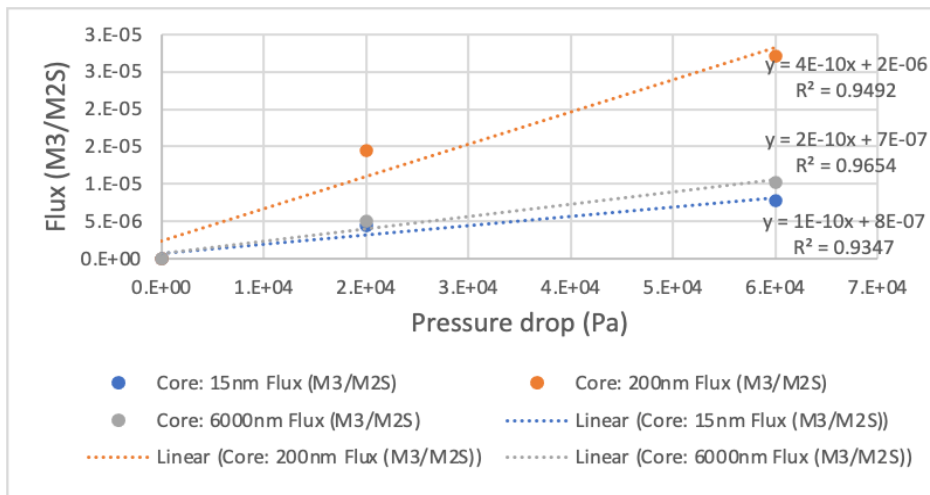Figure 12. Effect of Pressure Drop on Flux for the Different Membranes at Temperature 100° at the Darcy's Region

Figure 13. Effect of Pressure Drop on Flux for the Different Membranes at Temperature 150° at the Darcy's Region
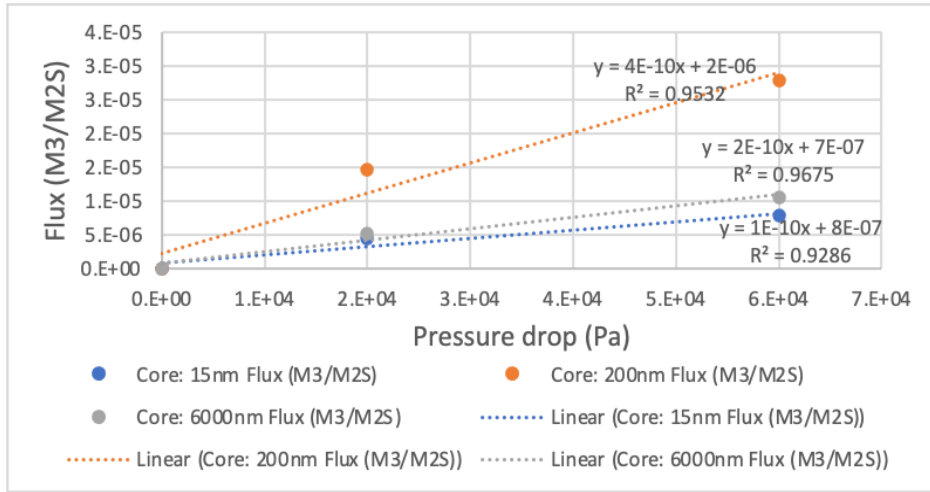
Figure 14. Effect of Pressure Drop on Flux for the Different Membranes at Temperature 200° at the Darcy's Region
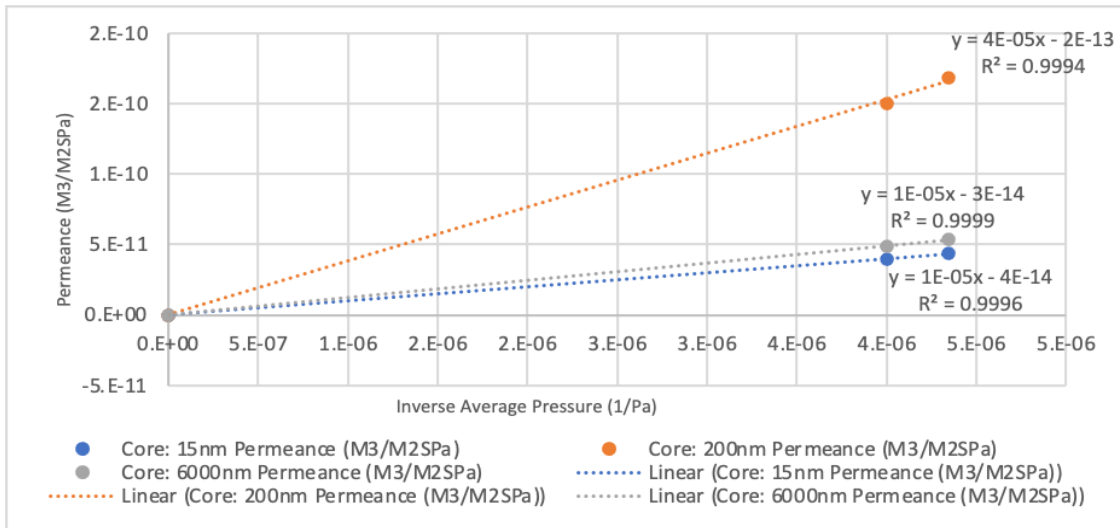

Figure 15. Effect of Inverse Average Pressure on Permeance for the Different Membranes at Temperature 100° at the Darcy's Region

Figure 16. Effect of Inverse Average Pressure on Permeance for the Different Membranes at Temperature 150° at the Darcy's Region

Figure 17. Effect of Inverse Average Pressure on Permeance for the Different Membranes at Temperature 200° at the Darcy's Region
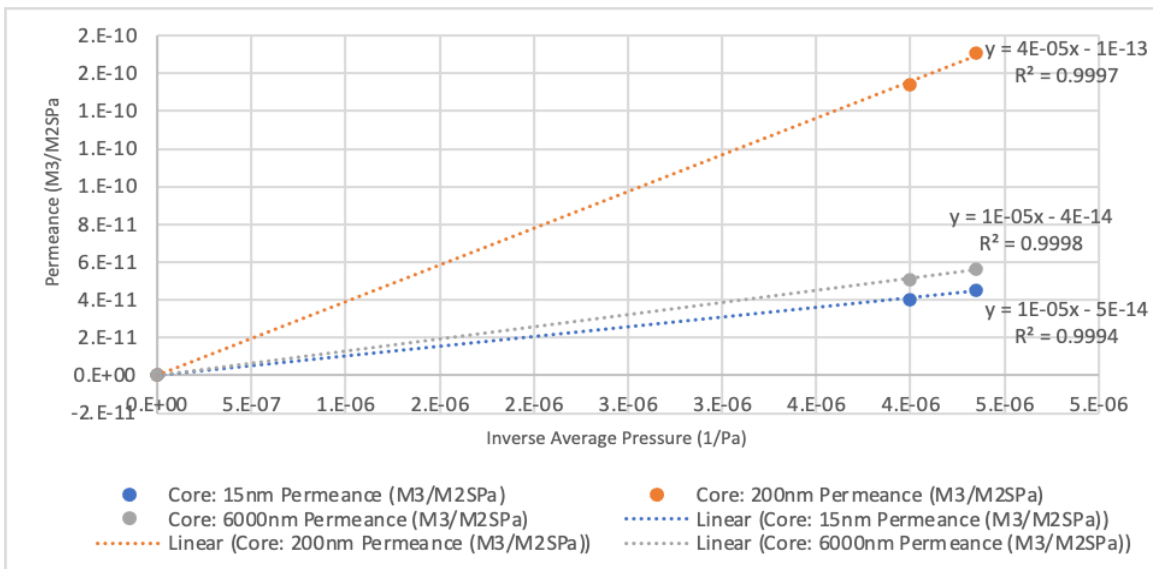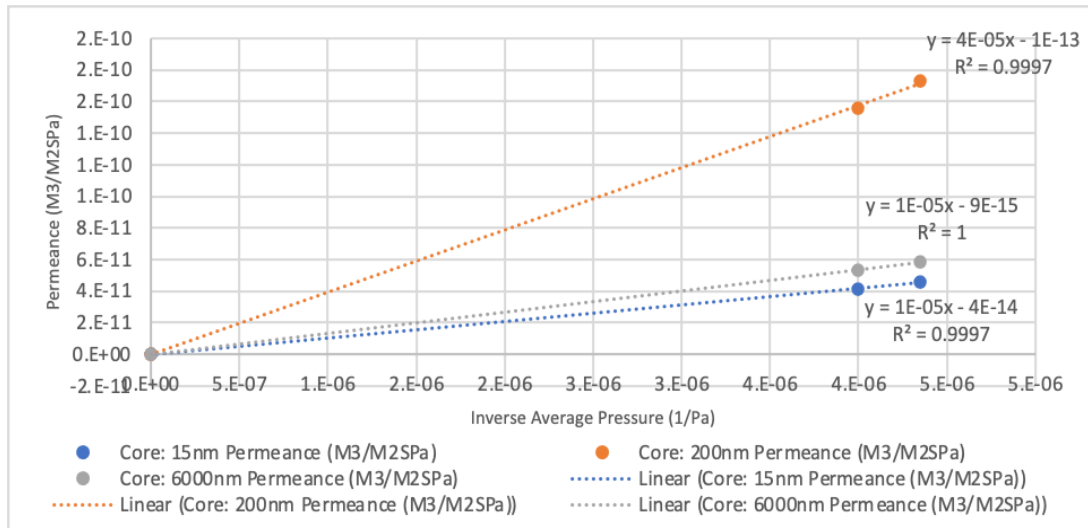
Discussion

In gas transport phenomena, flux is the rate of flow of gas per unit area, where the area is the surface area of the medium in which the gas is flowing through. Previous works reveal that under lamina flow conditions, pressure drop is proportional to volumetric flowrate. Pressure drop increases as gas viscosity increases. Fluid flow needs a pressure differential between points in which flow is directly proportional to the pressure gradient. Higher pressure differences will give a greater flowrate.

Predetermined pressures ranging from 0.2 to 3.0bar at 0.4bar increment intervals were used to conduct the experiment for three different membranes of pore sizes; 15nm, 200nm and 6000nm at different temperatures. From the statistical plots in figure 3, 4 and 4, temperature of 100°C, 150°C and 200°C was adopted for all three membranes to buttress the effect of pressure drop on the flux. The plots indicate how natural gas behaves when there is a change in pressure. As the pressure increases from 0.2bar to 3bar, the gas tends to move faster thereby increasing the rate at which it flows per unit area in the system regardless of the temperature difference. The result from the experiments confirms that as the reservoir pressure increases the reservoir permeability also increases, which means pressure gradient establishes the direction and rate of flow of gas in a reservoir.

In figure 6, 7 and 8 the average pressure was considered and plotted against the permeance, which is the measure of the degree to which the membrane allow gas to permeate. From the plots, as the average pressure increases the permeance tends to degrees. Apparent permeability of rocks samples increases gradually with decrease of average pressure. The increase is gentle when the average pressure is higher than 5MPa and becomes steeper when the average pressure is lower. The average pressure changes by nearly an order of magnitude. The flow pattern of shale gas is slippage flow because of the small Knudsen number.

In Figures 9, 10 and 11 the effect of inverse average pressure on permeance for the different membranes at different temperature was studied to demonstrate what happens when the average pressure values are inverted. From the plot as the inverse average pressure increases the capacity to which the membranes allow gases to permeate increases.

In Figures 12, 13 and 14 the effect of the pressure drop on flux for the different membranes at different temperatures was considered in the Darcy region. The variation of CH$_4$ fluxes as a function of applied transmembrane pressure for the different membranes at various pressure drops (ΔP) confirms Darcy's Law. Under Darcy flow the velocity (v) of a fluid traveling through a porous medium is directly proportional to the pressure gradient, $\Delta P/\delta$ (a difference in pressure ΔP over some finite distance δ), and inversely proportional to the viscosity of the fluid or gas, μ. The flow of gas through a porous membrane is based on two concepts— transport mechanism e.g., Darcy flow through the porous medium and component material balance. In Darcy flow the proportionality constant κ, is called the Darcy permeability, and is used to characterize the porous medium. Thus, the Darcy formula for linear displacement is given by equation 2: (Whitaker, 1986).

$$q/A = Q = -\kappa \Delta P / \mu \delta \qquad (2)$$

Where:

q = fluid volumetric flowrate, $m^3 s^{-1}$

A = cross-sectional area of the porous medium perpendicular to the flow, m^2

Q = fluid Volume flux, $m^3 \, m^{-2} s^{-1}$

κ = absolute permeability, m^2

ΔP = pressure difference (Pa) across the distance parallel to the direction of flow.

μ = the fluid viscosity, Pa-s

δ = finite distance, m

The flux Q was plotted against the pressure drop ΔP *with the slop of the graph equals* $-\kappa/\mu\delta$

In Figures 15, 16 and 17 the effect of the inverse of mean pressure on permeance for the different membranes at different temperatures studied in the Darcy region was considered. Intrinsic permeability represents the mobility of fluid within porous materials and solely related to pore geometry of the material itself (porosity, pore shape and pore size distribution etc.), and is independent of property of the fluid. Therefore, intrinsic permeability measured by any gas as pore fluid in a laboratory test should be same with that measured by any kind of fluids. Permeability is functions of both medium and a fluid property, and its relationship to intrinsic permeability is given by

$$K = k\rho g/\eta \qquad (3)$$

Where:

K is permeability (hydraulic conductivity) (m/s),

k is intrinsic permeability (m2),

η is viscosity of fluid (Pa·s),

ρ is fluid density (kg/m3),

g is gravitational acceleration (m/s2).

Equation (3) indicates that fluid mobility depends on both fluid viscosity and density. Permeability was measured in this study by the steady-state flow method by establishing differential pore pressure. In Fig. 15, 16 and 17 the permeability to methane gas is plotted against the inverse of the average pore pressure, Pav, to confirm Klinkenberg effect (Klinkenberg, et al 1941) effect. For most cases, permeability to gas increases linearly with an increase of 1/Pav, and this is consistent with Klinkenberg equation on the assumption that average pore pressure is equivalent to pore pressure. Permeability to water can be estimated from the slopes of the plots in Figure 15, 16 and 17.

Conclusion and Further Work

Unlike conventional gas reservoirs, gas flow in shale reservoirs is a complex and multiscale flow process which has special flow mechanisms. Shale gas reservoirs contain a large fraction of nano pores, which leads to an apparent permeability that is dependent on pore pressure, fluid type, and pore structure. Therefore, study of gas flow in nano pores is essential for accurate numerical simulation of shale gas reservoirs. However, no comprehensive study has been conducted pertaining to the gas flow in nano pores. In this paper, experiments for methane flow through nano membranes (with pore throat size: 15nm, 200nm, and 6000 nm) have been done and analyzed. Obvious discrepancy between apparent permeability and intrinsic permeability has been observed; and the relationship between this discrepancy and pore throat diameter (PTD) has been analyzed. The effect of the pore size on the behaviour of the gas was analysed, and the results obeyed the criteria to divide the flow stage into Darcy and Non-Darcy flow.

Based on the advection-diffusion model, further works will be done, and a new mathematical model will be constructed to characterize gas flow in nano pores. A new apparent permeability expression will be derived based on advection and Knudsen diffusion. A comprehensive coefficient for characterizing the flow process will be proposed. Simulation results will be verified against the experimental data for gas flow through nano membranes and published data. The model will be verified using experimental data with different gases (oxygen, argon) and different PTDs. A comparison will be made to show that the new model matches the experimental data very closely. Additionally, the results will be compared with experimental data, the Knudsen/Hagen–Poiseuille analytical solution, and existing models available in the literature. Water permeability experiments are planned in the future to confirm Klinkenberg slip factor and compare the K values obtained from water transport measurements. This work will provide a solid foundation for later research on gas flow in shale strata and numerical simulation in nanotubes.

Acknowledgements

References

Bird R.B., Steward W.E., and Lightfoot E.N. (2002) *transport phenomena.* 2nd edn. New York, USA. John Wiley & sons Inc 2002.

Bustin R.M., (2006) *where are the high potential regions expected to be in Canada and U.S. capturing opportunities in Canada shale gas.* Second annual shale gas conference. The Canadian institute, Calgary. January 31 – February 1.

Cramer D.D. (2008) *stimulating unconventional reservoirs:lesson learned, successful practices, areas for improvement.* SPE paper No. 114172. Proceedings of the unconventional gas conference. Keystone, February 10-12.

Hildenbrand A.A., Ghanizadeh A. and Krooss B,M, (2012) *transport properties of unconventional gas systems. Marine and petroleum geology. Vol 31, pp 90-99. 1 March.*

Javadpour F. and Difisher M. (2007) *nano-scale gas flow in shale sediment.* Journal of Canadian petroleum technology (46) pp 55-61.

Klinkenberg, L. J.: The permeability of Porous media to liquids and gases, American Petroleum Institute Drilling and Productions Practices, 200–213, 1941.

Martini, A.M., K., and Petsch S.T. (2004) *enhancing microbial gas from unconventional reservoirs: geochemical and microbial characterization of methane rich fractured black shale*. Final report, subcontract. No R,520 GRI 05/0023. Research partnership to source energy for human. Washington DC.

Speight J. G. (2013) *natural gas, a basic handbook.* GPC books, Gulf publishing company, Houston. TX

Siddharth G., Arnab K. P, Ravi K., and Archana M. N., 2019. A comprehensive analysis on the relationship between elastic wave velocities and petrophysical properties of sedimentary rocks based on laboratory measurements. *Journal of petroleum exploration and production technology 9, 1869-1881.*

Sunjay M.K., and Govind M. (2019) *diffusion process in gas reservoir system.* Conference paper, geophysics BHU, Varanasi 221005. India june 01.

Yao J., Sun H., Fan D., Wang C., and Sun Z. (2013) *numerical simulation of gas transport mechanism in tight shale gas reservoirs.* Journal of petroleum science, Berjin (10) pp 528-537.

Yu C, Ji S, Li Q., 2016. *Effects of porosity on seismic velocities, elastic moduli and Poisson's ratios of solid materials and rocks*. J Rock Mech Geotech Eng 8:35– 49.

Whitaker, S., 1986. *Flow in porous media I: A theoretical derivation of Darcy's law*. Transport in Porous Media.1: 3–25.

Ziarani A.S., and Hguilera R. (2012) *knudsen's permeability correction for tight porous media. Transport in porous media.* 91(1) pp 239-260.